Chemosphere 193 (2018) 664–674

Contents lists available at ScienceDirect

Chemosphere

journal homepage: www.elsevier.com/locate/chemosphere

New particle formation and growth at a suburban site and a background site in Hong Kong

X.P. Lyu [a, b], H. Guo [a, b, *], H.R. Cheng [c, **], D.W. Wang [d]

[a] Department of Civil and Environmental Engineering, The Hong Kong Polytechnic University, Hong Kong
[b] Research Institute for Sustainable Urban Development, The Hong Kong Polytechnic University, Hong Kong
[c] Department of Environmental Engineering, School of Resource and Environmental Sciences, Wuhan University, Wuhan, China
[d] State Key Laboratory of Atmospheric Boundary Layer Physics and Atmospheric Chemistry, Institute of Atmospheric Physics, Chinese Academy of Sciences, Beijing, China

HIGHLIGHTS

- Regional transport elevated the concentration of nanoparticles in Hong Kong.
- Cluster activation theory explained most new particle formation events in Hong Kong.
- Ozonolysis of α-pinene contributed to formation and growth of nucleation mode particles.

ARTICLE INFO

Article history:
Received 4 September 2017
Received in revised form
10 November 2017
Accepted 13 November 2017
Available online 14 November 2017

Handling Editor: Dr. R Ebinghaus

Keywords:
Atmospheric nanoparticle
New particle formation
Particle growth
Sulfuric acid vapor
Volatile organic compound

ABSTRACT

Atmospheric nanoparticles have great impacts on human health and global climate change. The number concentrations and size distributions of nanoparticles in the size range of 5.5–350.4 nm were detected at a background site and a suburban site in Hong Kong from summer to winter in 2011 and in autumn of 2013, respectively. Significantly higher particle number concentrations in all modes were observed at the suburban site ($p < 0.05$) during the sampling periods, possibly due to stronger primary emissions/regional transport and more intensive new particle formation (NPF). Particle number concentrations were much enhanced under northerly winds at both sites, resulting from regional transport of Aitken and accumulation mode particles, enhanced local NPF and occasionally low condensation sink. NPF was mainly limited by the precursors of condensable vapors and oxidative capacity of the atmosphere at the background site and the suburban site, respectively. In most cases, the formation rate of 5.5 nm particles was a function of sulfuric acid vapor to the power of 1.32 ± 0.34 at the background site and 0.81 ± 0.31 at the suburban site, abiding by the cluster activation theory. However, ozonolysis of monoterpenes (particularly α-pinene) might also drive NPF, particularly in the afternoon. These reactions also contributed to the growth of nucleation mode particles, which was largely explained by sulfuric acid vapor (73.6 ± 10% at the background site and 60.4 ± 9.8% at the suburban site). In contrast, the oxidations of isoprene, β-pinene and aromatics (particularly xylenes and trimethylbenzenes) were found to participate in the growth of Aitken mode particles.

1. Introduction

Nanoparticles (with aerodynamic diameter <350 nm) are ubiquitous in the atmosphere, and they interact with global climate change and pose harm to human health (Seaton et al., 1995; Seinfeld and Pandis, 2016). Combustion processes, such as vehicular exhaust and biomass burning, have been identified as the direct sources of nanoparticles (Petters et al., 2009; Ronkko et al., 2007, 2017). New particle formation (NPF) is a widely recognized source of secondary nanoparticles in atmosphere, spanning from the clean afforested areas in Europe to the highly polluted cities in China (Kulmala et al., 2006 and references therein). Both the

* Corresponding author. Department of Civil and Environmental Engineering, The Hong Kong Polytechnic University, Hong Kong.
** Corresponding author.
E-mail addresses: ceguohai@polyu.edu.hk (H. Guo), chenghr@whu.edu.cn (H.R. Cheng).

https://doi.org/10.1016/j.chemosphere.2017.11.060
0045-6535/

primarily emitted and secondarily formed particles can grow up to size of 50–100 nm, acting as cloud condensation nuclei (CCN) in the atmosphere (Gunthe et al., 2009). It is estimated that NPF globally contributes up to 50% of the atmospheric CCN (Spracklen et al., 2008; Trostl et al., 2016).

So far, the generally recognized NPF goes through the processes of nucleation of gaseous vapors which form molecular clusters, and the growth of clusters to the detectable sizes or even larger particles (Kulmala et al., 2005). Condensable vapors, such as sulfuric acid and organic condensable vapors generated from the oxidation of sulfur dioxide (SO_2) and volatile organic compounds (VOCs), respectively (Sihto et al., 2006; Trostl et al., 2016), play critical roles in both nucleation and particle growth. During NPF, the newly formed particles are also lost through coagulation and further growth into larger size particles (Kulmala et al., 2001; Dal Maso et al., 2002). Therefore, intensive NPF events were always observed in pristine environments where the condensation sinks were weak (*e.g.*, 0.02–0.025 s^{-1}) with low concentration of pre-existing particles in the atmosphere (Weber et al., 1997; Allan et al., 2006; Modini et al., 2009). However, recent observations in China clearly identified NPF processes in the heavily polluted environments with the condensation sink up to ~0.1 s^{-1} (Xiao et al., 2015). This likely implied different mechanisms in terms of nucleation and particle growth. Cluster activation theory and kinetic nucleation have been proposed to illustrate the nucleation mechanisms of sulfuric acid (Kulmala et al., 2006; Yu, 2006). However, these theories are occasionally not adequate to explain the observed particle formation rate. For example, either of them cannot interpret the intensive NPF processes observed during a dust event in China (Nie et al., 2014). Although the alternative particle formation mechanisms, like uptake of photochemical oxidants and heterogeneous reactions on dust surface, were suspected, the exact nucleation mechanisms are still unknown or left to be verified (Nie et al., 2014). Recently, the base-stabilization mechanism has been known to account for a great fraction of particle formation rates in the atmosphere. Specifically, either ammonia of 100 pptv or dimethylamine of 3 pptv could enhance the particle formation rates by up to 1000 folds, due to the significant reduction of acid vapor evaporations (Kirkby et al., 2011; Almeida et al., 2013). For particle growth, both sulfuric acid and organic condensable vapors are believed to be critical contributors, while the relative importance of them needs to be identified in different cases (Boy et al., 2005; Trostl et al., 2016). On the other hand, particle growth is generally size dependent ruled by Kelvin effect (smaller particles have higher Kelvin barrier, requiring higher saturation ratio of condensable vapors to drive particle growth). Therefore, the roles of sulfuric acid and organic condensable vapors in particle growth may be also size dependent. For example, Trostl et al. (2016) indicated that the saturation concentration of organic vapors that contributed to growth of nucleated particles should be less than $10^{-4.5}$ μg/m^3. In addition, Lehtipalo et al. (2016) indicated that particle growth was accelerated by the bases that were capable of stabilizing sulfuric acid clusters (*e.g.* ammonia and dimethylamine). As such, further studies are necessary to advance our understanding on the formation and growth of atmospheric nanoparticles.

Hong Kong is a subtropical megacity on the coast of South China Sea (SCS), adjoining the fast-developing Pearl River Delta (PRD) region in South China. The geographical location makes it a unique place to study NPF, because it is influenced by both clean air from SCS and dirty air laden with SO_2 and VOCs from PRD (Guo et al., 2009; Jiang et al., 2010). In addition, the vehicle density in Hong Kong is among the highest over the world, implying that local emissions of nanoparticles and their precursors are also considerable. Although our previous studies (Guo et al., 2012; Wang et al., 2014) observed the NPF and particle burst events at a mountainous and an urban site in Hong Kong, the roles of SO_2 and VOCs in particle formation and growth are not well recognized. This study focused on the formation and growth of nanoparticles at two contrastive sites in Hong Kong. The relationships of sulfuric acid vapor and the formation rates of first-generation oxidation products of VOCs (proxies of organic condensable vapors, as discussed below) with NPF were explored.

2. Methodology

2.1. Site description

Field measurements of nanoparticles, VOCs and trace gases were carried out from September 17 to November 22, 2013 at Tung Chung (TC) in southwestern Hong Kong. To the northwest of the site (22.29° N, 113.94° E) is the Pearl River Estuary where PRD originated air pollutants often accumulate (Wang et al., 2003; Zheng et al., 2010). The site is located in the downwind area of urban Hong Kong and city clusters in the PRD region in cold season (October–March) under prevailing northeasterly winds. In warm season (April–September) southerly winds originating from SCS dominate at the site, diluting air pollution. The potential local sources of air pollutants around this site include the Hong Kong international airport (HKIA, ~3 km to the northwest), a nearby airport highway and the residential activities. Previous study indicated that the impact from the airport on VOCs levels at TC was insignificant (Guo et al., 2007; https://www.hongkongairport.com/eng/sustainability/environmental-management/DraftAOAQSReport.pdf), recently further confirmed by the Environmental Impact Assessment Report for Expansion of Hong Kong International Airport into a Three-Runway system (http://www.epd.gov.hk/eia/register/report/eiareport/eia_2232014/html/Ch%205%20-%20Air%20Quality.pdf). Industrial and vehicular emissions in Hong Kong and PRD were the main sources of VOCs. In addition, TC is a newly developed residential town with few industries and less dense transportation. Hence, it was defined as a suburban site in previous studies (Guo et al., 2009). Field measurements were also conducted at a Hok Tsui (HT) in August, November and December 2011. This site (22.22° N, 114.25° E) is at the tip of southeastern Hong Kong, facing SCS and having very sparse anthropogenic sources. Therefore, it has served as a background site in Hong Kong for decades (Lee et al., 2002; Wang et al., 2009). Fig. 1 shows the geographical location of both sites.

2.2. Field measurements

Atmospheric particle number concentrations in the size range of 5.5–350.4 nm were monitored by a Scanning Mobility Particle Sizer (SMPS) coupled with a butanol-based Condensation Particle Counter (Grimm, model 5.400, Germany) at both sites. Particles were counted in 44 size bins every 4 min, according to their mobility in a differential mobility analyzer mounted in the SMPS. The air was drawn into the instrument through a 1.5 m conductive tube (ID: 0.8 cm), and the particle diffusion losses in the tubing were taken into account in the data analysis. To guarantee the data quality, the instrument was operated following the protocols introduced in Wang et al. (2014). It should be noted that about half of the data were missing for the measurements at both TC and HT, due to instrumental maintenance.

Concentrations of SO_2, carbon monoxide (CO), ozone (O_3), nitric oxide (NO) and nitrogen dioxide (NO_2) at TC were downloaded from the website of Hong Kong Environmental Protection Department (HKEPD, http://epic.epd.gov.hk/EPICDI/air/station/). The data were checked by a quality system in accordance with the Hong

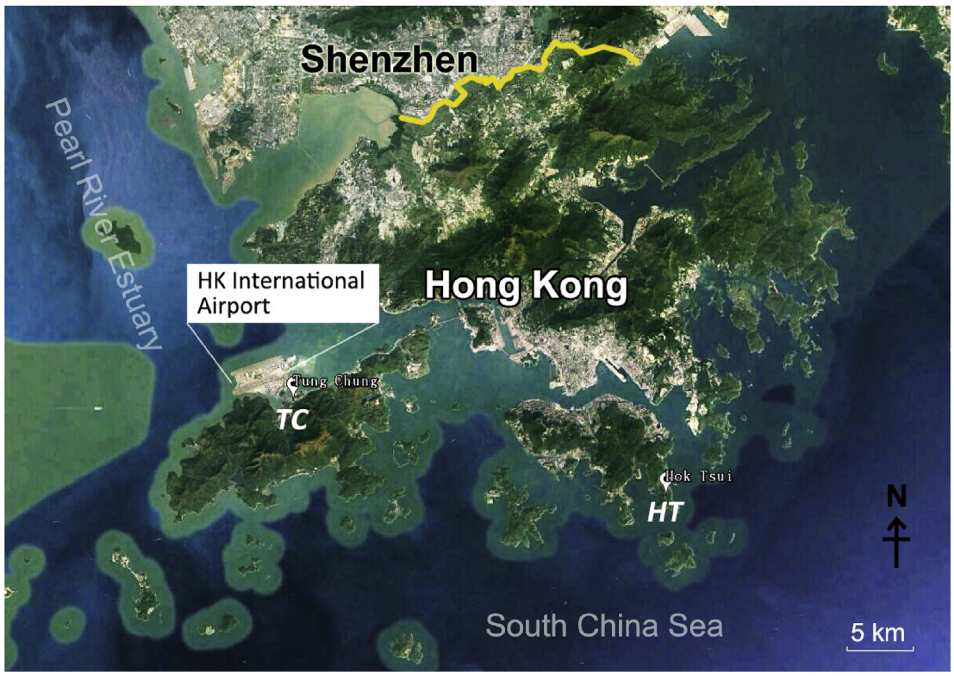

Fig. 1. Geographical location of the sampling sites. The border between mainland China and Hong Kong is highlighted in yellow. (For interpretation of the references to colour in this figure legend, the reader is referred to the web version of this article.)

Kong Laboratory Accreditation Scheme criteria. In 2013 (the year when the data at TC were used in this study), the accuracy and precision of trace gases measurements were <12% and 6.1%, respectively (HKEPD, 2013). The trace gases were continuously monitored at HT by ourselves. A transfer standard (Thermal Environmental Instruments, 49PS) was used to calibrate the O_3 analyzer. In addition, the measurements of SO_2, CO and NO were calibrated using a NIST (National Institute of Standards and Technology) - traceable standard, which contains 156.5 ppmv CO (±2%), 15.64 ppmv SO_2 (±2%), and 15.55 ppmv NO (±2%). NO_2 measurement was not calibrated, because NO_2 was converted to NO through a converter containing heated molybdenum, and was measured in the form of converted NO. Details about the instruments, measurement techniques and detection limits at both sites are provided in Table S1. VOCs were also measured at both sites, which are detailed in Text S1. The trace gas analyzers used at the two sites were the same, except for the O_3 analyzer which however had highly comparable measurement results during the intercomparison in our laboratory. For VOC analysis, the on-line and off-line methods were compared during the sampling campaign at TC in autumn of 2013. Good agreements of the speciated VOCs were found between the two methods with R^2 of 0.7–0.9 and slope of 0.7–1.1 (Fig. S1 shows examples of the comparison between the on-line and off-line VOCs). The on-line instrument for VOC analysis at HT was identical to that at TC. Further, the same SMPS was utilized to detect particle number distributions at TC and HT. Therefore, the different brands of instruments and analysis techniques would not hamper the comparisons of air pollutants between the two sites.

2.3. Processing of SMPS data

In this study, nanoparticles in the size range of 5.5–350.4 nm detected by SMPS were divided into particles in nucleation mode (5.5–24.7 nm), Aitken mode (24.7–101.4 nm) and accumulation mode (101.4–350.4 nm). To study NPF processes, the formation rate of 5.5 nm particles ($J_{5.5}$), condensation sink (CS) and the productions of condensable vapors were calculated. Details about the calculations can be found in Text S2. All the statistical data shown in this study were in form of mean ± 95% confidence interval, unless otherwise specified.

3. Results and discussion

3.1. Overall characteristics of nanoparticles at HT and TC

Figs. 2–3 show hourly average particle number concentrations (PNs, cm^{-3}) in modes of nucleation (PN_{Nuc}), Aitken (PN_{Ait}) and accumulation (PN_{Acc}) during the sampling periods at HT and TC, respectively. Also shown are the wind fields, total volatile organic compounds (TVOCs), O_3, SO_2, CO, NO and NO_2 in hourly resolution. The average wind speed at HT (4.7 ± 0.2 m/s) was much higher than that at TC (1.1 ± 0.1 m/s; $p < 0.05$), since it adjoins SCS and has very few buildings around. More frequent (43.9%) northerly ($0° < WD < 90°$ and $270° < WD < 360°$) winds were monitored at HT, compared to 32.0% at TC. Temperature and relative humidity at HT during the sampling period were also higher (not shown here), likely biased by the data collected in summer (August), in contrast to the data collected in autumn at TC (September–November).

Overall, the average concentrations of air pollutants (inorganic trace gases and TVOCs) were lower at HT ($p < 0.05$). PN_{Nuc}, PN_{Ait} and PN_{Acc} at HT was (1.4 ± 0.1) × 10^3, (5.5 ± 0.3) × 10^3 and (1.5 ± 0.1) × 10^3 cm^{-3}, respectively. In comparison, the PNs at TC were significantly higher than those at HT ($p < 0.05$), with PN_{Nuc}, PN_{Ait} and PN_{Acc} of (6.1 ± 0.6) × 10^3, (6.7 ± 0.4) × 10^3 and (2.4 ± 0.1) × 10^3 cm^{-3}, respectively. The total PNs at TC ((14.3 ± 0.2) × 10^3 cm^{-3}) was nearly twice that at HT ((7.8 ± 0.1) × 10^3 cm^{-3}). Fig. S2 presents detailed statistics of the total PNs and PNs in different modes at the two sites. Since Hong Kong is a highly developed city with relatively stable construction activities, vehicle population, and forestation rate, the variations of inter-annual emissions of nanoparticles and their precursors were not expected as the main cause of the different levels of air

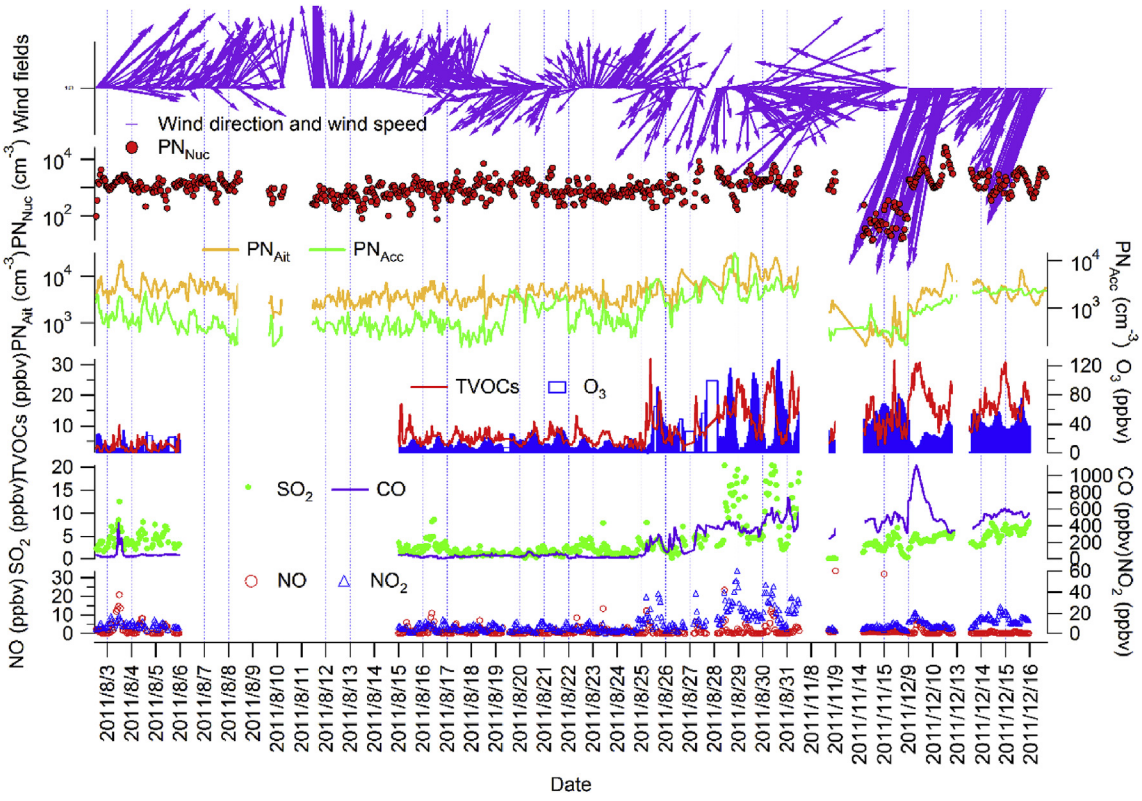

Fig. 2. Hourly average wind fields, PN_{Nuc}, PN_{Ait}, PN_{Acc}, TVOCs, O_3, SO_2, CO, NO and NO_2 at HT. The horizontal axis is not continuous for the dates in November and December due to instrumental maintenance.

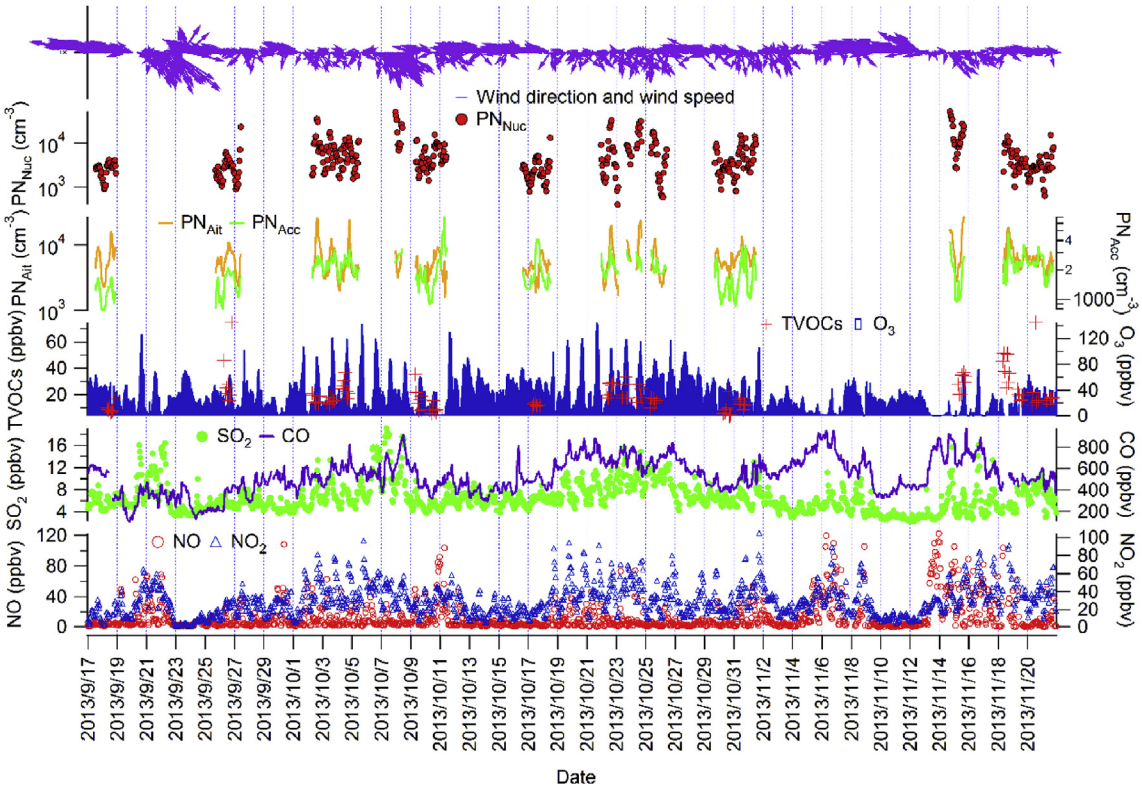

Fig. 3. Hourly average wind fields, PN_{Nuc}, PN_{Ait}, PN_{Acc}, TVOCs, O_3, SO_2, CO, NO and NO_2 at TC. PNs and TVOCs are not consecutive because they were collected only on selected high O_3 days and low O_3 days in order to study photochemistry.

pollutants and PNs between the two sites. This was confirmed by the stable levels of trace gases ($p > 0.05$) through January 2011 to December 2013 measured at TC by HKEPD (Fig. S3). Furthermore, Table S2 compares the mixing ratios of trace gases concurrently monitored at TC and HT during August–December 2011. Noticeably, all the pollutants had higher levels at TC ($p < 0.05$), except for the lower O_3 due to titration by fresh emission of NO, implying that the regional transport and/or primary emission of air pollutants including nanoparticles might be more significant at TC. Namely, the higher PNs at TC were not caused by the different sampling periods but the different land-use features between the two sites. In addition, the NPF potential at TC might be stronger in view of higher SO_2, TVOCs and O_3, which also partially explained the higher PNs at this suburban site. The NPF events at both sites were distinguished by sudden increase of PN_{Nuc}, which lasted for no less than 1 h. Meanwhile, the primary air pollutants should not increase significantly. A parameter reflecting the relative abundance of nucleation mode particles (PN_{Nuc}/UFP, UFP means ultrafine particles with diameters less than 100 nm) was also used to further identify the NPF events with a threshold of PN_{Nuc}/UFP>0.5 (Jung et al., 2013; Peng et al., 2017). In total, 14 out of 35 days (40%) and 13 out of 26 days (50%) were identified as NPF days at HT and TC, respectively. Moreover, the proportions of PNs in each mode of total PNs were calculated. While PN_{Ait}/PNs and PN_{Acc}/PNs were comparable to or even lower than those at HT, the fraction of PN_{Nuc} in total PNs (PN_{Nuc}/PNs) at TC (33.3 ± 0.3%) was much higher than that (16.0 ± 0.2%) at HT. The more frequent NPFs at TC might be partially responsible for the higher PNs and the higher ratio of PN_{Nuc}/PNs. Furthermore, the lower fraction of PN_{Nuc}/PNs at HT could be caused by growth and/loss of nucleation mode particles during the transport of air masses to this background site.

It was found that PNs generally increased under northerly winds at both sites. To clearly show the relationships between PNs and wind sectors, Table 1 summarizes the average PNs in three modes and total PNs under different wind fields. Clearly, PNs were remarkably higher under northeasterly and northwesterly winds ($p < 0.05$), except for the relatively high concentrations of Aitken and accumulation mode particles under southwesterly winds. Since HT is a background site, the higher PNs under northerly winds implied the transport of nanoparticles or particle precursors to the site. This is reasonable for Aitken and accumulation mode particles, because to the north of the site are the urban areas of Hong Kong and city clusters of PRD with high potentials of nanoparticle emission and formation. For example, in late August 2011, the typhoon “Nanmadol” brought air masses from inland PRD to this site. PN_{Ait} and PN_{Acc} increased remarkably, so did the gas-phase air pollutants. The enhancements of primary air pollutants (*e.g.*, TVOCs, SO_2, CO and NO) suggested the transport of primarily emitted particles. However, the enhancement of PN_{Nuc} at HT was not attributable to regional transport or even transport from the urban areas of Hong Kong, because the time for air mass traveling from inland PRD (>2 h) and urban Hong Kong (>30 min) to the site was generally longer than the scavenging time (~20 min) of nucleation mode particles through growth and coagulation (Ronkko et al., 2017 and references therein). This was also confirmed in section 3.2 (*i.e.*, no daytime peak for PN_{Nuc}, in contrast to the peaks for larger size particles due to transport during non-NPFs). It was found that O_3, TVOCs and SO_2 were generally elevated under northerly winds (*e.g.*, August 28–31, 2011 at HT). Therefore, the higher PN_{Nuc} might be caused by the enhanced local NPFs. Another example is the much higher PN_{Nuc} on December 9–10, 2011, when Hong Kong was under the dominance of a continental anticyclone and very strong northeasterly winds prevailed (average wind speed = 11.7 ± 0.3 m/s). Particularly on December 10 when obvious NPF was observed, PN_{Nuc} reached the highest level throughout the sampling campaign. Differing from their elevated concentrations in late August, the gas-phase air pollutants stayed at relatively low levels on these two days, expect for TVOCs and CO on December 09, implying that the increase of PN_{Nuc} could not be explained by primary emissions. The atmospheric oxidative capacity was also not very strong, in view of the moderate levels of O_3 (maximum = 43.8 ppbv). However, we found that condensation sink was very low on these two days (CS~0.014 s^{-1}), possibly due to the scavenging of the preexisting aerosol particles by strong winds. The low CS favored the survival of newly formed particles, resulting in high PN_{Nuc}. During the increase of PNs at HT under northerly winds, it was likely that PNs at TC were more elevated, which however could not be discussed here due to lack of concurrent observation data.

At TC, regional transport of air pollutants under northerly winds has been confirmed by a number of studies (*e.g.*, Hagler et al., 2006; Guo et al., 2009), which might enhance PN_{Ait} and PN_{Acc} levels at this site. However, as discussed earlier, the enhancement of PN_{Nuc} could only be attributed to local NPF driven by increased concentrations of gas-phase air pollutants, because the nucleation mode particles could not survive for such a long-distance transport. In fact, both SO_2 and O_3 at TC increased substantially under northerly winds (not shown), which likely facilitated the local NPFs. Therefore, it could be concluded that high PNs under northerly winds were resulted from the transport of Aitken and accumulation mode particles, the enhancement of local NPF and/or occasionally low CS benefited from the strong winds.

3.2. Comparison between NPF and non-NPF

As discussed earlier, NPF might be an important factor leading to high PNs at both sites. Table 2 compares the PNs, gas-phase air pollutants and solar radiation during NPFs and non-NPFs. It was

Table 1
Average particle number concentrations in nucleation, Aitken and accumulation modes in different wind sectors (Unit: $cm^{-3} \times 10^3$).

	Wind sector	PN_{Nuc}	PN_{Ait}	PN_{Acc}	Total PN
Summer (August) at HT	NE	1.7 ± 0.3	4.9 ± 0.4	1.8 ± 0.2	5.4 ± 0.5
	SE	0.9 ± 0.1	3.9 ± 0.3	1.0 ± 0.1	4.1 ± 0.3
	SW	1.0 ± 0.1	5.6 ± 0.4	1.0 ± 0.1	5.8 ± 0.4
	NW	1.5 ± 0.2	9.7 ± 1.3	3.0 ± 0.6	10.3 ± 1.4
Autumn and winter (November and December) at HT	NE	2.3 ± 0.6	4.5 ± 0.6	1.7 ± 0.2	5.3 ± 0.9
	SE	0.1 ± 0.03	0.8 ± 0.2	0.3 ± 0.04	0.9 ± 0.2
	SW	–	–	–	–
	NW	–	–	–	–
Autumn (September–November) at TC	NE	8.2 ± 1.2	6.8 ± 0.6	2.4 ± 0.1	10.9 ± 1.3
	SE	2.8 ± 0.2	5.4 ± 0.3	2.1 ± 0.1	6.4 ± 0.4
	SW	5.2 ± 0.5	6.1 ± 0.7	2.7 ± 0.2	8.5 ± 0.9
	NW	14.9 ± 2.5	11.1 ± 1.3	2.9 ± 0.1	18.8 ± 2.8

Table 2
Average particle number concentrations and mixing ratios of gas-phase air pollutants during NPF and non-NPF at HT and TC. Bold fonts denote significant differences between NPF and non-NPF ($p < 0.05$).

	HT		TC	
	NPF	Non-NPF	NPF	Non-NPF
PN_{Nuc} ($cm^{-3} \times 10^3$)	**2.1 ± 0.1**	**1.0 ± 0.02**	**6.7 ± 0.2**	**5.1 ± 0.2**
PN_{Ait} ($cm^{-3} \times 10^3$)	**6.4 ± 0.2**	**4.9 ± 0.1**	**7.3 ± 0.2**	**6.1 ± 0.1**
PN_{Acc} ($cm^{-3} \times 10^3$)	**1.6 ± 0.04**	**1.4 ± 0.04**	2.4 ± 0.02	2.4 ± 0.03
SO_2 (ppbv)	**4.8 ± 0.5**	**3.5 ± 0.3**	6.9 ± 0.3	7.0 ± 0.3
TVOCs (ppbv)	**12.3 ± 1.0**	**8.0 ± 0.6**	19.5 ± 2.3	17.4 ± 3.8
O_3 (ppbv)	28.0 ± 3.2	26.6 ± 2.2	35.6 ± 3.4	36.7 ± 2.2
NO_2 (ppbv)	**12.1 ± 1.2**	**9.4 ± 0.8**	**35.0 ± 1.8**	**27.7 ± 2.1**
NO (ppbv)	1.3 ± 0.2	1.6 ± 0.4	13.7 ± 2.1	10.5 ± 2.1
CO (ppbv)	**320.9 ± 35.0**	**178.6 ± 19.5**	537.5 ± 15.2	522.6 ± 17.3
Solar radiation (W/m^2)	341.9 ± 37.7	333.2 ± 33.5	**364.9 ± 41.6**	**254.7 ± 37.3**
Qsa ($molecules/cm^3$)	**(7.4 ± 1.1) × 10^6**	**(5.3 ± 0.9) × 10^6**	**(16 ± 2.8) × 10^6**	**(7.9 ± 1.7) × 10^6**

found that PNs in all modes increased significantly ($p < 0.05$) during NPFs, except for the unchanged PN_{Acc} at TC ($p > 0.05$). As the precursors of condensable vapors, SO_2 and TVOCs were also elevated during NPFs at HT, which might accelerate the formation and growth of nanoparticles and resulted in higher PNs. For example, the estimated Qsa was higher during NPFs (7.4 ± 1.1 × 10^6 molecules/cm^3) than during non-NPFs (5.3 ± 0.9 × 10^6 molecules/cm^3) at HT, with the comparable solar radiation. In addition, higher level of CO (320.9 ± 35.0 ppbv) was observed during NPFs, compared to that (178.6 ± 19.5 ppbv) during non-NPFs. However, no study has reported the promotion of CO to NPF. The increase of CO during NPFs at HT was likely caused by regional transport of air masses laden with SO_2 and TVOCs, which facilitated NPFs at the site. In contrast, SO_2, TVOCs and CO were all comparable ($p > 0.05$) between NPFs and non-NPFs at TC, indicating that the precursor of condensable vapors was not the limiting factor of NPF at this site. This might be due to the fact that the concentrations of gas-phase air pollutants were relatively high at TC, which were sufficient in producing the condensable vapors. Note that the solar radiation was much stronger during NPFs at TC. Consequently, the estimated Qsa during NPFs at TC (16 ± 2.8 × 10^6 molecules/cm^3) was nearly twice that during non-NPFs (7.9 ± 1.7 × 10^6 molecules/cm^3), despite comparable SO_2. The results demonstrated the importance of atmospheric oxidative capacity in NPF at TC, because SO_2 was readily oxidized to sulfuric acid by photochemical reactions. Furthermore, NO_2 increased significantly ($p < 0.05$) during NPFs at both HT and TC, while NO remained stable ($p > 0.05$). The inconsistent variations of NO and NO_2 indicated that the increase of NO_2 during NPFs was not attributable to primary emissions, but secondary formation. Therefore, the total oxidant (O_x, $O_x = O_3 + NO_2$) was used to represent the oxidative capacity of the atmosphere. O_x increased from 64.3 ± 1.7 ppbv during non-NPFs to 70.6 ± 3.8 ppbv during NPFs at TC, while it remained statistically unchanged ($p > 0.05$) at HT (36.0 ± 2.4 and 40.1 ± 3.6 ppbv during non-NPFs and NPFs, respectively). As such, we assume that NPFs at the background site (HT) were mainly limited by the precursors of condensable vapors, while the oxidative capacity of the atmosphere was the dominant factor of NPFs at the suburban site (TC).

Fig. 4 plots the average diurnal patterns of PNs, O_3, SO_2 and TVOCs during NPFs and non-NPFs at HT and TC. During NPFs at HT (Fig. 4(a)), SO_2 and TVOCs were on relatively high levels at night. In the morning, PN_{Nuc} began to increase at 06:00, followed by the increase of PN_{Ait} 2 h later. Correspondingly, the peak of PNs shifted from 12:00 for nucleation mode particles to 14:00 for Aitken mode particles. NPFs might be driven by the photo-oxidations of SO_2 and TVOCs after sunrise. In contrast, the continuous increase of PN_{Nuc} in the morning was not observed for non-NPFs at HT (Fig. 4(b)). Instead, PN_{Nuc} sustained on high levels from the late afternoon (17:00) to the early morning (08:00), while it decreased to low levels between 09:00 and 16:00. This pattern was opposite to the diurnal variations of PN_{Ait}, PN_{Acc}, CO, SO_2 and TVOCs which had broad daytime peaks during non-NPFs (CO is not shown here). Since HT is a background site, the broad daytime peaks of these species might relate to regional transport. However, the low PN_{Nuc} in daytime indicated that nucleation mode particles were scavenged during the transport of air masses. In addition, the local processes, including particle growth, coagulation and development of boundary layer led to the decrease of PN_{Nuc} in daytime. Further, the relatively high level of PN_{Nuc} in the morning and evening rush hours during non-NPFs at HT coincided with the increases of NO and NO_2 in these hours (not shown here), implying the vehicular emissions of nucleation mode particles. Actually, the vehicular emission of nucleation mode particles and even smaller clusters has been reported in previous studies (Wehner et al., 2002; Ronkko et al., 2007, 2017). However, it should be noted that the vehicular emissions were more likely local but not regional. Despite a background site, there might still be some vehicle activities in the surrounding area.

The diurnal variations of PN_{Nuc} and PN_{Ait} during NPFs at TC were similar to those during NPFs at HT. Differently, two small peaks were recorded for them in the periods of 05:00–08:00 and 17:00–20:00, parallel to the substantial increases of NO and NO_2 (not shown here). This implied the vehicular emissions of nucleation and Aitken mode particles at TC. Note that, the evening peaks were much higher than the morning peaks. We also noticed that the ratio of NO_2/NO between 17:00 and 20:00 (10.6 ± 2.9) was remarkably higher than that between 5:00 and 08:00 (2.5 ± 0.6) ($p < 0.05$). Since the compositions of vehicle exhausts were generally consistent, a great part of NO_2 in the evening rush hours was expected to be secondarily formed under the condition of high O_3 in the afternoon. Therefore, we suspect that the higher evening peaks of PN_{Nuc} and PN_{Ait} might also be caused by NPFs driven by O_3. However, this assumption needs to be verified in future study. Overall, during NPFs, PN_{Nuc} and PN_{Ait} elevated by vehicular emissions were lower than those ascribed to NPFs from morning to early afternoon, suggesting that NPF was still the dominant contributor to nucleation and Aitken mode particles during NPFs at TC. This circumstance was reversed during non-NPFs, when PN_{Nuc} peaked in morning and evening rush hours, elevated by the vehicular emissions. Although PN_{Ait} had a peak in the afternoon (13:00–15:00), we infer that this might be caused by the growth of nucleation mode particles emitted from vehicles in the morning.

In fact, the observed PNs are the results of competition between the formation and losses of particles. Therefore, the relationships

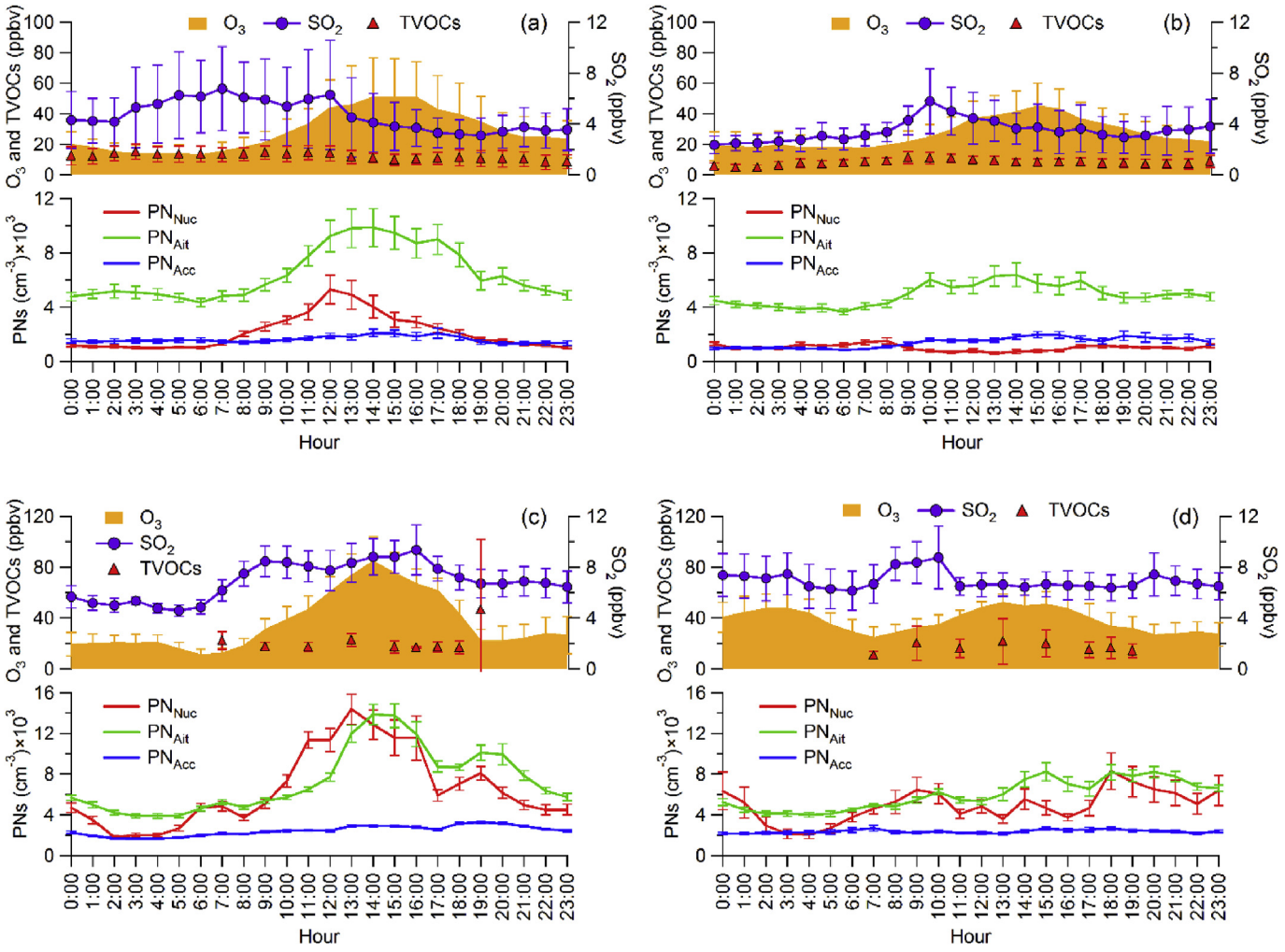

Fig. 4. Average diurnal patterns of PNs, O_3, SO_2 and TVOCs during (a) NPFs at HT, (b) non-NPFs at HT, (c) NPFs at TC and (d) non-NPFs at TC.

between particle formation potential and CS, an important loss pathway for nanoparticles (Dal Maso et al., 2002), were explored. In accordance with previous studies (Petaja et al., 2009; Nie et al., 2014), SR × SO_2 (SR: solar radiation) and O_3 were used to represent the particle formation potentials through the nucleation and condensation of sulfuric acid and condensable organic vapors, respectively. Fig. 5 shows the scatter plots between SR × SO_2 and CS, as well as O_3 and CS, at HT and TC. It was found that CS was comparable between 0.017 ± 0.002 s^{-1} during non-NPFs and 0.019 ± 0.002 s^{-1} during NPFs at HT ($p > 0.05$). SR × SO_2 and O_3 also remained statistically stable ($p > 0.05$). However, the ratios of SR × SO_2/CS and O_3/CS increased ($p < 0.05$) from (61.0 ± 1.8) × 10^3 W/m^2·ppbv/s^{-1} and 1139 ± 12 ppbv/s^{-1} during non-NPFs to (86.4 ± 2.3) × 10^3 W/m^2·ppbv/s^{-1} and 1539 ± 13 ppbv/s^{-1} during NPFs, respectively. This might explain higher PNs during NPF events at HT, because the net production of nanoparticles increased with the integrated consideration of the formation and loss processes. At TC, more discrete relationships were found between the proxies of particle formation potential (*i.e.* SR × SO_2 and O_3) and CS. However, from non-NPF to NPF, the average SR × SO_2 and O_3 significantly increased by ~45% and ~21% ($p < 0.05$), respectively, compared to the insignificant enhancement ($p > 0.05$) of CS (from 0.021 ± 0.002 s^{-1} to 0.025 ± 0.002 s^{-1}, ~14%). Therefore, the net productions of nanoparticles also increased during NPFs at TC, resulting in higher PNs.

3.3. Possible mechanisms of NPF

Previous studies (Boy et al., 2005; Kulmala et al., 2006) indicated that sulfuric acid, produced from the photo-oxidation of SO_2, played important roles in nucleation and particle growth. To understand the effects of sulfuric acid on NPFs in Hong Kong, the relationships between the formation rate of 5.5 nm particles ($J_{5.5}$) and the estimated concentration of sulfuric acid vapor (Q_{sa}) were studied. Generally, the particle formation rate is a power function of sulfuric acid with the power index between 1 and 2, when time delay between the formation of sulfuric acid and new particles is appropriately applied (Kulmala et al., 2006; Sihto et al., 2006). Fig. 6 plots the logarithm of $J_{5.5}$ against the logarithm of Q_{sa} at HT and TC, with the time delay between $J_{5.5}$ and Q_{sa} varying from 1 to 3 h. To minimize the influence of primary emissions, $J_{5.5}$ was calculated between 09:00 and 16:00 at both sites. On average, $J_{5.5}$ at TC (2.5 ± 0.5 cm^{-3} s^{-1}) was significantly higher than at HT (0.6 ± 0.1 cm^{-3} s^{-1}) ($p < 0.05$), suggesting more intensive NPFs at the suburban site. This might be explained by the higher concentration of SO_2, TVOCs and O_3 at TC (see Table 2). For example, as a result of higher SO_2, the estimated sulfuric acid during daytime (07:00–19:00) at TC (4.1 ± 0.5 × 10^7 molecules·cm^{-3}) was more than twice that at HT (1.9 ± 0.3 × 10^7 molecules·cm^{-3}), which might more efficiently promote NPFs at TC. According to Fig. 6, the power index between $J_{5.5}$ and Q_{sa} were much lower than 1 at both

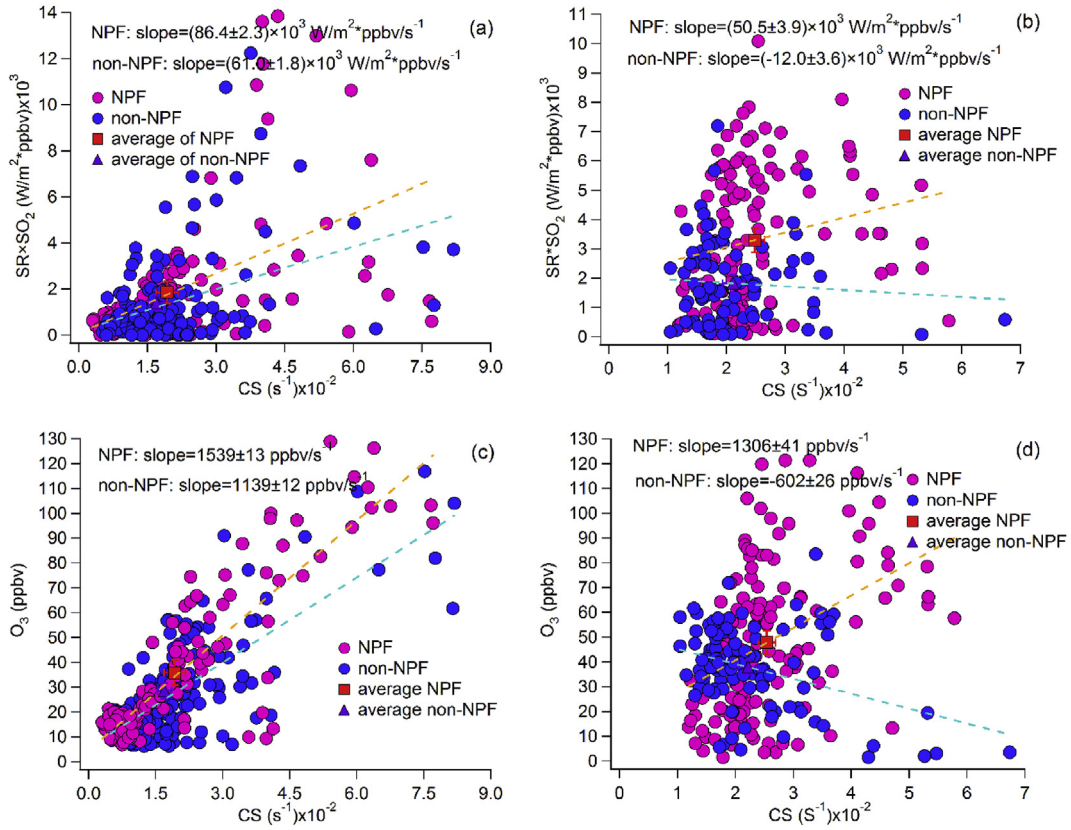

Fig. 5. Relationship between SR × SO_2 and CS at (a) HT and (b) TC; between O_3 and CS at (c) HT and (d) TC. SR denotes solar radiation.

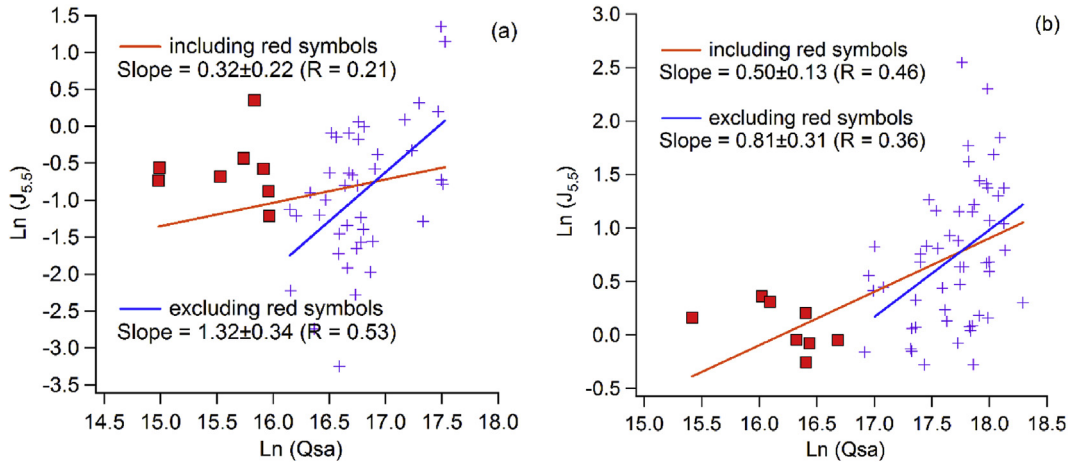

Fig. 6. Linear regression between Ln ($J_{5.5}$) and Ln (Q_{sa}) at (a) HT and (b) TC. Red symbols represent samples significantly deviated from the majorities. (For interpretation of the references to colour in this figure legend, the reader is referred to the web version of this article.)

HT (0.32 ± 0.22) and TC (0.50 ± 0.13), inconsistent with many previous studies (*e.g.* Kulmala et al., 2006; Sihto et al., 2006), including our own previous findings at a mountainous site (power index: 1.3; Guo et al., 2012) and an urban site (power index: 2.8; Wang et al., 2014) in Hong Kong. This indicated that the formation of particles at both sites cannot be explained by either the cluster activation theory (power index = 1) or kinetic mechanism (power index = 2). However, we found that some data points significantly deviated from the majorities, as shown in red symbols in Fig. 6. These samples featured relatively low concentrations of sulfuric acid, but had higher particle formation rates than expected. When excluding these samples in regression analysis, the power index between $J_{5.5}$ and Q_{sa} became comparable to 1, *i.e.*, 1.32 ± 0.34 at HT and 0.81 ± 0.31 at TC. Namely, the cluster activation theory proposed by Kulmala et al. (2006) could explain most NPF events at both sites. The dependence of $J_{5.5}$ on Q_{sa}, particularly for the deviated values, might be influenced by many factors, such as temperature, relative humidity and the concentration of bases (*e.g.* ammonia and amine).

Interestingly, all the samples excluded from the linear regression at HT were observed at 15:00–16:00, meaning that NPFs in these hours might be explained by other mechanisms or caused by

condensable vapors other than sulfuric acid. At TC, three of the eight excluded samples were observed at 16:00. Further insight into the variation of $N_{5.5\text{-}10}$ (a determinant parameter of $J_{5.5}$) found that $N_{5.5\text{-}10}$ increased slightly in the afternoon on some days (*e.g.*, December 10 and 15, 2011 at HT and October 2–3, 2013 at TC). Moreover, the increases of $N_{5.5\text{-}10}$ in the afternoon were always accompanied by or immediately followed the peak of O_3. As examples, Fig. 7 shows the variations of $N_{5.5\text{-}10}$, PN_{Acc} and other gas-phase air pollutants throughout December 10, 2011 at HT and October 3, 2013 at TC. Increases of $N_{5.5\text{-}10}$ were observed between 14:26 and 15:16 in the former case, and between 16:14–17:19 in the latter case, with the rate of 804 and 1057 $cm^{-3}\ h^{-1}$, respectively. During the enhancements of $N_{5.5\text{-}10}$, PN_{Acc} showed the decreasing trends in both cases (rate = -188 and −160 $cm^{-3}\ h^{-1}$, respectively). In addition, the gas-phase air pollutants also decreased except for the increases of SO_2 in the former case and TVOCs in the latter case. Although SO_2 increased between 13:00 and 15:00 in the former case, the estimated sulfuric acid decreased in this period, due to the weakened solar radiation (Fig. 7(a)). All these signatures implied that the increases of $N_{5.5\text{-}10}$ in the afternoon were not caused by primary emissions or NPFs driven by sulfuric acid. Furthermore, while the enhancement of $N_{5.5\text{-}10}$ was accompanied by the decrease of CS ($p < 0.05$) in the latter case, the CS remained stable ($p = 0.32$) during the increase of $N_{5.5\text{-}10}$ in the former case (Fig. S4), indicating that the elevation of $N_{5.5\text{-}10}$ in the afternoon was not exclusively caused by the lowering of CS. This phenomenon was also occasionally observed at a mountainous site in Hong Kong in 2010, as shown in Fig. S5 (PN_{Nuc} is presented to replace $N_{5.5\text{-}10}$ due to the big fluctuations of $N_{5.5\text{-}10}$ in that sampling campaign) (Guo et al., 2012). It is noteworthy that O_3 were on the highest levels before or during the increases of $N_{5.5\text{-}10}$ in these cases. By the inspiration that ozonolysis of α-pinene participates in NPF (Hoffmann et al., 1998; Bonn and Moorgat, 2002), we infer that ozonolysis of VOCs might be responsible for the buildup of the 5.5–10 nm nanoparticles in the afternoon.

To verify this hypothesis, the productions of condensable vapors proxies (see section 2.3) at TC were compared between the excluded (red square) and included samples (purple cross) in Fig. 6. Since time was needed for nucleation and for particles to grow up to the detectable size (≥5.5 nm), the proxies productions in 3 h ahead of the observation of each sample were considered in calculation of the proxies productions for the samples. Table S3 lists the pathway-specified productions of proxies of organic condensable vapors in these two cases. It was found that proxies production through ozonolysis of α-pinene for the excluded samples ($2.2 \pm 0.3 \times 10^4$ molecules/cm^3/s) was significantly higher than that for the included samples ($1.5 \pm 0.3 \times 10^4$ molecules/cm^3/s) ($p < 0.05$), while the productions through other pathways were comparable ($p > 0.05$). This suggested that condensable vapors produced from "O_3+α-pinene" might dominate NPF at TC in some cases. Furthermore, the correlations between $J_{5.5}$ and the pathway-specified proxies of condensable vapor productions at TC were examined, with suitable time delays of 1–3 h(s), as shown in Table 3. Noticeably, $J_{5.5}$ had moderate correlations with proxies productions through ozonolysis of α-pinene (R = 0.44) and β-pinene (R = 0.49), in addition to the moderate correlation with Q_{sa} (R = 0.48). It therefore can be concluded that O_3 oxidation of monoterpenes (including α-pinene and β-pinene) played important roles in NPFs at TC. In view of the comparable productions of condensable vapors through O_3+ β-pinene between the excluded and included samples (see Table S3), this pathway might not be the

Table 3
Correlation coefficients (R) of $J_{5.5}$ and the differences between calculated and observed GR versus pathway-specified proxies of condensable vapor productions at TC. Bold font denotes moderate correlations (R ≥ 0.40).

Pathway	$J_{5.5}$	$\triangle GR_{Nuc}$	$\triangle GR_{Ait}$
OH + isoprene	0.003	0.25	**0.48**
O_3 + isoprene	0.25	−0.10	**0.41**
OH + α-pinene	0.23	0.39	0.37
O_3 + α-pinene	**0.44**	**0.78**	0.11
OH + β-pinene	0.14	0.14	**0.46**
O_3 + β-pinene	**0.49**	−0.24	**0.44**
OH + benzene	0.19	−0.08	0.33
OH + toluene	0.27	−0.21	0.30
OH + ethylbenzene	0.27	−0.18	0.39
OH + xylenes	0.29	−0.16	**0.46**
OH + trimethylbenzenes	0.35	−0.21	**0.45**
Q_{sa}	**0.48**	0.21	0.11

The aromatics were chosen according to the availability and completeness of the data.

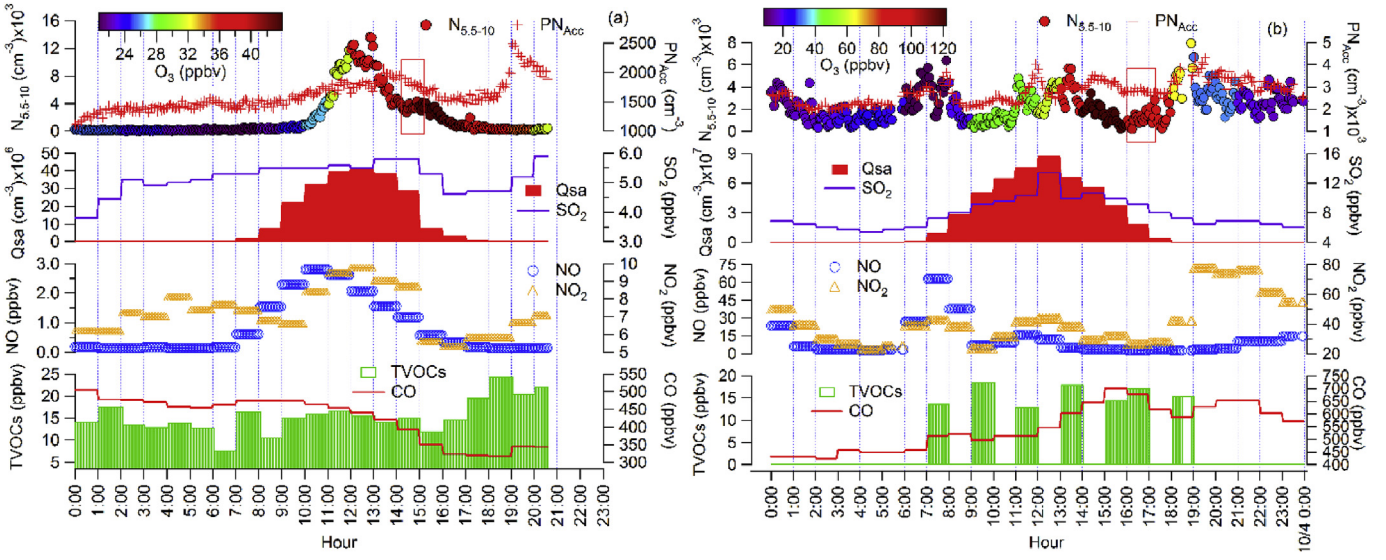

Fig. 7. Diurnal variations of $N_{5.5\text{-}10}$, PN_{Acc} and gaseous air pollutants on (a) December 10, 2011 at HT and (b) October 3, 2013 at TC. Color of the $N_{5.5\text{-}10}$ symbols represents O_3 concentrations as indicated by the color scale. Gas-phase air pollutants are presented in hourly averages limited by the data resolutions. Increases of $N_{5.5\text{-}10}$ in the afternoon of interest are highlighted in red box. (For interpretation of the references to colour in this figure legend, the reader is referred to the web version of this article.)

main cause of $N_{5.5\text{-}10}$ increases in the afternoon, but participated in NPFs in other time of the day. Since monoterpene concentrations were not available at HT, the same conclusion cannot be directly drawn at that site. However, O_3 was much higher ($p < 0.05$) for the excluded samples (47.5 ± 15.8 ppbv) than the included samples (24.6 ± 4.8 ppbv), implying high potential of VOCs oxidation by O_3 for the excluded samples.

In addition to participating in nucleation, sulfuric acid and organic condensable vapors also accelerate particle growth. Therefore, growth rates of particles in nucleation (GR_{Nuc}) and Aitken modes (GR_{Ait}) were calculated and compared with the growth rates that can be attributable to sulfuric acids (GR_0). GR_0 was calculated based on the estimated sulfuric acid concentrations, with the consideration of hydration effect, according to Nieminen et al. (2010). It should be noted that GR_0 generally increased non-linearly with particle size increasing. Fig. S6 presents the observed GR_{Nuc}, GR_{Ait} and calculated GR_0 at HT and TC. Overall, as indicated by the fractions of GR_0 in GR_{Nuc} and GR_{Ait}, sulfuric acid could be responsible for 73.6 ± 10% and 60.4 ± 9.8% of GR_{Nuc} at HT and TC, respectively. These values were much higher than 9.2–52.5% reported by Guo et al. (2012) at a mountainous site in Hong Kong, as well as 5–30% in Europe summarized by Nieminen et al. (2010). The reason for this is that SO_2 concentration during NPFs at TC (6.9 ± 0.1 ppbv) was significantly higher than that at the mountainous site (4.5 ± 0.2 ppbv) ($p < 0.05$) (Guo et al., 2012), implying higher concentrations of sulfuric acid in the atmosphere. HT is a background site, where VOCs might be less abundant than the mountainous site, particularly the reactive biogenic VOCs. The lower concentrations of these VOCs might cause the lower contribution of VOCs to GR, resulting in higher fraction of GR explained by sulfuric acid. With particle size enlarging, sulfuric acid was only responsible for 29.6 ± 10.1% of GR_{Ait} at HT and 24.9 ± 8.5% of GR_{Ait} at TC, implying that other condensable vapors made great contribution to the growth of Aitken mode particles. The oxidation products of VOCs are the most possible alternatives according to previous studies (Kulmala et al., 2001; Riipinen et al., 2012).

To identify the roles of specific VOC oxidation pathways in particle growth, we subtracted GRs attributable to sulfuric acid from the observed GRs, getting the differences of GR for nucleation mode ($\triangle GR_{Nuc}$, $\triangle GR_{Nuc} = GR_{Nuc} - GR_0$) and Aitken mode particles ($\triangle GR_{Ait}$, $\triangle GR_{Nuc} = GR_{Ait} - GR_0$). Note that GR_0 was different for nucleation and Aitken mode particles (Nieminen et al., 2010). The correlations between $\triangle GR$ and the pathway-specified proxies production of organic condensable vapors at TC were examined (Table 3). Moderate correlations were found between $\triangle GR_{Nuc}$ and the ozonolysis of α-pinene ($R = 0.78$), likely indicating the stimulation of ozonolysis of α-pinene in growth of nucleation mode particles. However, the correlations became worse between α-pinene oxidation and $\triangle GR_{Ait}$. Instead, $\triangle GR_{Ait}$ correlated better with the oxidations of isoprene, β-pinene and aromatics (xylenes and trimethylbenzenes), with $R \geq 0.40$. This indicated that more VOCs participated in the growth of Aitken mode particles. The size-dependent roles of different VOCs in particle growth might relate to the volatilities of their oxidation products. Ruled by Kelvin effect, the smaller particles are more difficult to grow due to the higher vapor pressure on their surface. Therefore, organic vapors with lower volatilities are needed for the growth of smaller particles. Ozonolysis of α-pinene is widely recognized source of extremely low volatility organic vapors (Ehn et al., 2014; Trostl et al., 2016). Therefore, it was capable of involving in the growth of nucleation mode particles. However, for the growth of larger particles (*e.g.*, Aitken mode particles), the requirement for the non-volatilities of condensable vapors lowered and the oxidation products of more VOCs with higher volatilities could accelerate the particle growth.

4. Conclusions

Field measurements of airborne nanoparticles and gaseous air pollutants were carried out at a background site from summer to winter in 2011 and at a suburban site in autumn of 2013 in Hong Kong, respectively. Particle number concentrations in all modes were significantly higher at the suburban site than at the background site, due to higher vehicular emissions and more intensive NPFs. Regional transport under northerly winds greatly elevated particle number concentrations at both sites. For nucleation mode particles, the increase was mainly due to enhanced local NPFs driven by the regionally transported gas-phase air pollutants, which were precursors of condensable vapors. Also, under strong northerly winds, CS might decrease substantially, resulting in higher concentrations of nanoparticles. The precursors of condensable vapors and oxidative capacity of the atmosphere were found to be the main limiting factor of NPFs at the background site and the suburban site, respectively. The effect on NPF of the formations of sulfuric acid and organic condensable vapors overrode the scavenging of particles through condensation during NPFs at both sites, leading to higher net production of nanoparticles and increased particle number concentrations during NPFs. Most of the NPF events at both sites could be explained by the cluster activation theory. However, ozonolysis of α-pinene might dominate NPFs in some cases, particularly in the afternoon when O_3 was high. In addition, although sulfuric acid accounted for the major fraction of the growth of nucleation mode particles, ozonolysis of α-pinene played a non-negligible role in this process. With the particle size increment, the contribution of sulfuric acid to particle growth rate decreased, possibly leaving a higher fraction of growth rate attributable to organic condensable vapors generated from VOCs oxidation. The preliminary results indicated that VOCs including isoprene, β-pinene and aromatics (particularly xylenes and trimethylbenzenes) participated in the growth of Aitken mode particles. This study advanced our knowledge on NPF and growth in Hong Kong, which particularly demonstrated the importance of VOCs in airborne nanoparticle pollution in this region.

Acknowledgements

This study was supported by the Research Grants Council of the Hong Kong Special Administrative Region via grants CRF/C5004-15E, PolyU5154/13E, PolyU152052/14E, PolyU152052/16E and CRF/C5022-14G, and the Research Institute for Sustainable Urban Development of Hong Kong Polytechnic University (1-BBW4). This study is partly supported by the Hong Kong PolyU internal grant (G-YBHT, 1-ZVJT and 4-ZZFW) and the National Natural Science Foundation of China (No. 41275122).

Appendix A. Supplementary data

Supplementary data related to this article can be found at https://doi.org/10.1016/j.chemosphere.2017.11.060.

References

Allan, J.D., Alfarra, M.R., Bower, K.N., Coe, H., Jayne, J.T., Worsnop, D.R., Aalto, P.P., Kulmala, M., Hyotylainen, T., Cavalli, F., Laaksonen, A., 2006. Size and composition measurements of background aerosol and new particle growth in a Finnish forest during QUEST 2 using an Aerodyne Aerosol Mass Spectrometer. Atmos. Chem. Phys. 6 (2), 315–327.

Almeida, J., Schobesberger, S., Kurten, A., et al., 2013. Molecular understanding of sulphuric acid-amine particle nucleation in the atmosphere. Nature 502 (7471), 359–363.

Bonn, B., Moorgat, G.K., 2002. New particle formation during a-and b-pinene oxidation by O 3, OH and NO 3, and the influence of water vapour: particle size distribution studies. Atmos. Chem. Phys. 2 (3), 183–196.

Boy, M., Kulmala, M., Ruuskanen, T.M., Pihlatie, M., Reissell, A., Aalto, P.P., Keronen, P., Dal Maso, M., Hellen, H., Hakola, H., Jansson, R., Hanke, M., Arnold, F., 2005. Sulphuric acid closure and contribution to nucleation mode particle growth. Atmos. Chem. Phys. 5 (4), 863–878.

Dal Maso, M., Kulmala, M., Lehtinen, K.E., Makela, J.M., Aalto, P., O'Dowd, C.D., 2002. Condensation and coagulation sinks and formation of nucleation mode particles in coastal and boreal forest boundary layers. J. Geophys. Res. Atmos. 107 (D19).

Ehn, M., Thornton, J.A., Kleist, E., et al., 2014. A large source of low-volatility secondary organic aerosol. Nature 506 (7489), 476–479.

Guo, H., So, K.L., Simpson, I.J., Barletta, B., Meinardi, S., Blake, D.R., 2007. C1-C8 volatile organic compounds in the atmosphere of Hong Kong: overview of atmospheric processing and source apportionment. Atmos. Environ. 41, 1456–1472.

Guo, H., Jiang, F., Cheng, H.R., Simpson, I.J., Wang, X.M., Ding, A.J., Wang, T.J., Saunders, S.M., Wang, T., Lam, S.H.M., Blake, D.R., Zhang, Y.L., Xie, M., 2009. Concurrent observations of air pollutants at two sites in the Pearl River Delta and the implication of regional transport. Atmos. Chem. Phys. 9, 7343–7360.

Guo, H., Wang, D.W., Cheung, K., Ling, Z.H., Chan, C.K., Yao, X.H., 2012. Observation of aerosol size distribution and new particle formation at a mountain site in subtropical Hong Kong. Atmos. Chem. Phys. 12 (20), 9923–9939.

Gunthe, S.S., King, S.M., Rose, D., Chen, Q., Roldin, P., Farmer, D.K., Jimenez, J.L., Artaxo, P., Andreae, M.O., Martin, S.T., Poschl, U., 2009. Cloud condensation nuclei in pristine tropical rainforest air of Amazonia: size-resolved measurements and modeling of atmospheric aerosol composition and CCN activity. Atmos. Chem. Phys. 9 (19), 7551–7575.

Hagler, G.S.W., Bergin, M.H., Salmon, L.G., Yu, J.Z., Wan, E.C.H., Zheng, M., Zeng, L.M., Kiang, C.S., Zhang, Y.H., Lau, A.K.H., Schauer, J.J., 2006. Source areas and chemical composition of fine particulate matter in the Pearl River Delta region of China. Atmos. Environ. 40 (20), 3802–3815.

Hoffmann, T., Bandur, R., Marggraf, U., Linscheid, M., 1998. Molecular composition of organic aerosols formed in the α-pinene/O3 reaction: implications for new particle formation processes. J. Geophys. Res. Atmos. 103 (D19), 25569–25578.

HKEPD, 2013. Air Quality in Hong Kong 2013. accessible at. http://www.aqhi.gov.hk/en/download/air-quality-reportse469.html?showall=&start=1.

Jiang, F., Guo, H., Wang, T.J., Cheng, H.R., Wang, X.M., Simpson, I.J., Ding, A.J., Saunders, S.M., Lam, S.H.M., Blake, D.R., 2010. An ozone episode in the Pearl River Delta: field observation and model simulation. J. Geophys. Res. 115, D22305 https://doi.org/10.1029/2009JD013583.

Jung, J., Miyazaki, Y., Kawamura, K., 2013. Different characteristics of new particle formation between urban and deciduous forest sites in Northern Japan during the summers of 2010–2011. Atmos. Chem. Phys. 13 (1), 51–68.

Kirkby, J., Curtius, J., Almeida, J., et al., 2011. Role of sulphuric acid, ammonia and galactic cosmic rays in atmospheric aerosol nucleation. Nature 476 (7361), 429–433.

Kulmala, M., Lehtinen, K.E.J., Laaksonen, A., 2006. Cluster activation theory as an explanation of the linear dependence between formation rate of 3nm particles and sulphuric acid concentration. Atmos. Chem. Phys. 6 (3), 787–793.

Kulmala, M., Maso, M.D., Mäkelä, J.M., Pirjola, L., Väkevä, M., Aalto, P., Miikkulainen, P., Hameri, K., O'dowd, C.D., 2001. On the formation, growth and composition of nucleation mode particles. Tellus B Chem. Phys. Meteorol. 53 (4), 479–490.

Kulmala, M., Petäjä, T., Mönkkönen, P., Koponen, I.K., Maso, M.D., Aalto, P.P., Lehtinen, K.E.J., Kerminen, V.M., 2005. On the growth of nucleation mode particles: source rates of condensable vapor in polluted and clean environments. Atmos. Chem. Phys. 5 (2), 409–416.

Lee, S.C., Chiu, M.Y., Ho, K.F., Zou, S.C., Wang, X., 2002. Volatile organic compounds (VOCs) in urban atmosphere of Hong Kong. Chemosphere 48 (3), 375–382.

Lehtipalo, K., Rondo, L., Kontkanen, J., et al., 2016. The effect of acid–base clustering and ions on the growth of atmospheric nano-particles. Nat. Commun. 7, 11594.

Modini, R.L., Ristovski, Z.D., Johnson, G.R., He, C., Surawski, N., Morawska, L., Suni, T., Kulmala, M., 2009. New particle formation and growth at a remote, sub-tropical coastal location. Atmos. Chem. Phys. 9 (19), 7607–7621.

Nie, W., Ding, A., Wang, T., Kerminen, V.M., George, C., Xue, L., Wang, W., Zhang, Q., Petäjä, T., Qi, X., Gao, X., Wang, X., Yang, X., Fu, C., Kulmala, M., 2014. Polluted dust promotes new particle formation and growth. Sci. Rep. 4, 6634. https://doi.org/10.1038/srep06634.

Nieminen, T., Lehtinen, K.E.J., Kulmala, M., 2010. Sub-10 nm particle growth by vapor condensation–effects of vapor molecule size and particle thermal speed. Atmos. Chem. Phys. 10 (20), 9773–9779.

Peng, Y., Liu, X., Dai, J., Wang, Z., Dong, Z., Dong, Y., Chen, C., Li, X., Zhao, N., Fan, C., 2017. Aerosol size distribution and new particle formation events in the suburb of Xi'an, northwest China. Atmos. Environ. 153, 194–205.

Petaja, T., Mauldin Iii, R.L., Kosciuch, E., McGrath, J., Nieminen, T., Paasonen, P., Boy, M., Adamov, A., Kotiaho, T., Kulmala, M., 2009. Sulfuric acid and OH concentrations in a boreal forest site. Atmos. Chem. Phys. 9 (19), 7435–7448.

Petters, M.D., Carrico, C.M., Kreidenweis, S.M., Prenni, A.J., DeMott, P.J., Collett, J.L., Moosmueller, H., 2009. Cloud condensation nucleation activity of biomass burning aerosol. J. Geophys. Res. Atmos. 114 (D22) https://doi.org/10.1029/2009JD012353.

Riipinen, I., Yli-Juuti, T., Pierce, J.R., Petäjä, T., Worsnop, D.R., Kulmala, M., Donahue, N.M., 2012. The contribution of organics to atmospheric nanoparticle growth. Nat. Geosci. 5 (7), 453.

Ronkko, T., Kuuluvainen, H., Karjalainen, P., Keskinen, J., Hillamo, R., Niemi, J.V., Pirjola, L., Timonen, H.J., Saarikoski, S., Saukko, E., Jarvinen, A., Silvennoinen, H., Rostedt, A., Olia, M., Yli-ojanpera, J., Nousiainen, P., Kousa, A., Dal Maso, M., 2017. Traffic is a major source of atmospheric nanocluster aerosol. Proc. Natl. Acad. Sci. 114 (29), 7549–7554.

Ronkko, T., Virtanen, A., Kannosto, J., Keskinen, J., Lappi, M., Pirjola, L., 2007. Nucleation mode particles with a nonvolatile core in the exhaust of a heavy duty diesel vehicle. Environ. Sci. Technol. 41 (18), 6384–6389.

Seaton, A., Godden, D., MacNee, W., Donaldson, K., 1995. Particulate air pollution and acute health effects. lancet 345 (8943), 176–178.

Seinfeld, J.H., Pandis, S.N., 2016. Atmospheric Chemistry and Physics: from Air Pollution to Climate Change. John Wiley & Sons.

Sihto, S.L., Kulmala, M., Kerminen, V.M., Maso, M.D., Petaijai, T., Riipinen, I., Korhonen, H., Arnold, F., Janson, R., Boy, M., Laaksonen, A., Lehtinen, K.E.J., 2006. Atmospheric sulphuric acid and aerosol formation: implications from atmospheric measurements for nucleation and early growth mechanisms. Atmos. Chem. Phys. 6 (12), 4079–4091.

Spracklen, D.V., Carslaw, K.S., Kulmala, M., Kerminen, V.M., Sihto, S.L., Riipinen, I., Merikanto, J., Mann, G.W., Chipperfield, N., Wiedensohler, A., Birmili, W., Lihavainen, H., 2008. Contribution of particle formation to global cloud condensation nuclei concentrations. Geophys. Res. Lett. 35 (6) https://doi.org/10.1029/2007GL033038.

Trostl, J., Chuang, W.K., Gordon, H., et al., 2016. The role of low-volatility organic compounds in initial particle growth in the atmosphere. Nature 533 (7604), 527–531.

Wang, D.W., Guo, H., Cheung, K., Gan, F.X., 2014. Observation of nucleation mode particle burst and new particle formation events at an urban site in Hong Kong. Atmos. Environ. 99, 196–205.

Wang, T., Poon, C.N., Kwok, Y.H., Li, Y.S., 2003. Characterizing the temporal variability and emission patterns of pollution plumes in the Pearl River Delta of China. Atmos. Environ. 37 (25), 3539–3550.

Wang, T., Wei, X.L., Ding, A.J., Poon, S.C., Lam, K.S., Li, Y.S., Chan, L.Y., Anson, M., 2009. Increasing surface ozone concentrations in the background atmosphere of Southern China, 1994-2007. Atmos. Chem. Phys. 9, 6217–6227.

Weber, R.J., Marti, J.J., McMurry, P.H., Eisele, F.L., Tanner, D.J., Jefferson, A., 1997. Measurements of new particle formation and ultrafine particle growth rates at a clean continental site. J. Geophys. Res.: Atmos. 102 (D4), 4375–4385.

Wehner, B., Birmili, W., Gnauk, T., Wiedensohler, A., 2002. Particle number size distributions in a street canyon and their transformation into the urban-air background: measurements and a simple model study. Atmos. Environ. 36 (13), 2215–2223.

Xiao, S., Wang, M.Y., Yao, L., Kulmala, M., Zhou, B., Yang, X., Chen, J.M., Wang, D.F., Fu, Q.Y., Worsnop, D.R., Wang, L., 2015. Strong atmospheric new particle formation in winter in urban Shanghai, China. Atmos. Chem. Phys. 15 (4), 1769–1781.

Yu, F., 2006. Effect of ammonia on new particle formation: a kinetic H_2SO_4-H_2O-NH_3 nucleation model constrained by laboratory measurements. J. Geophys. Res. Atmos. 111 (D1) https://doi.org/10.1029/2005JD005968.

Zheng, J., Zhong, L., Wang, T., Louie, P.K., Li, Z., 2010. Ground-level ozone in the Pearl River Delta region: analysis of data from a recently established regional air quality monitoring network. Atmos. Environ. 44 (6), 814–823.